J. Eur. Opt. Society-Rapid Publ. 2024, **20**, 23

https://doi.org/10.1051/jeos/2024023
Available online at: https://jeos.edpsciences.org

Journal of the European Optical Society-Rapid Publications

RESEARCH ARTICLE OPEN ACCESS

Ultra low RIN, low threshold AlGaInAs/InP BH-DFB laser

Jianhua Ren[1], Yanhui Xing[1], Jun Han[1,*], Tianyu Sun[2,*], Zheng Xing[2], Can Yin[1], and Baoshun Zhang[2]

[1] Key Laboratory of Opto-electronics Technology, Ministry of Education, College of Microelectronics, Beijing University of Technology, Beijing 100124, PR China
[2] Nanofabrication Facility, Suzhou Institute of Nano-Tech and Nano-Bionics, Chinese Academy of Sciences, Suzhou 215123, PR China

Received 22 March 2024 / Accepted 25 April 2024

Abstract. This study presents a comparative analysis of AlGalnAs buried heterostructure laser diodes by using dual-channel ridge-waveguides. Different shaped channels, including bowl shaped groove and vertical groove, are explored. Using a vertical groove structure, we achieved an output power of 90 mW at 25 °C with a threshold current of only 4 mA. This represents a 3.6-fold increase in output power compared to the BH-DFB structure. At a high temperature of 85 °C, the laser maintains a side-mode suppression ratio of over 45 dB at the maximum power point. The laser's relative intensity noise in the 0–40 GHz frequency range is less than −162.8 dB/Hz when operated at 300 mA with the chip butterfly packaged. These findings underscore the robustness, reliability, and high-performance capabilities of the developed DFB laser, highlighting its potential for various practical applications.

Keywords: Laser, RIN, AlGaInAs, Trench.

1 Introduction

With the growing demand for enhanced signal transmission system performance, microwave photonic links are gaining popularity due to their significant bandwidth and low loss. With the growing applications of microwave photonic links in radar [1, 2], electronic warfare [3], and other fields, there is a strong emphasis on achieving the highest possible Spurious-Free Dynamic Range (SFDR) under broadband conditions. Lasers are the core components of microwave photonic links, and their Relative Intensity Noise (RIN) and optical power significantly affect the SFDR of the link.

Reducing the RIN of lasers has been studied extensively by many research groups. By optimizing the structure of the waveguide layer, it is possible to decrease the internal losses of the laser while simultaneously enhancing its internal quantum efficiency, thus facilitating the realization of low RIN and high-power Distributed Feedback (DFB) lasers. In 2003, Japan's Furukawa Electric [4] achieved a laser output of 175 mW with RIN less than −160 dB/Hz (1–2 GHz) utilizing an InGaAsP quantum well structure and a buried heterogeneity (BH). Subsequently, in 2018, Morton Photonics of the United States [5] accomplished a laser output of 101 mW with RIN less than −160 dB/Hz employing the InGaAsP quantum well structure and a ridge waveguide configuration.

Currently, the development of BH-DFB semiconductor lasers faces several challenges, notably the inadequate energy depth of quantum wells and a heightened risk of Auger recombination processes [6]. As the pumping current increases, carriers may flow out of the active region, resulting in leakage current and consequently reducing the quantum efficiency of the laser. Auger recombination further reduces radiative recombination, laser efficiency, and increases heat dissipation. I compared to InGaAsP, AlGaInAs exhibits a lower Auger recombination rate due to its larger conduction band offset difference [7], which enhances electron utilization, effectively reduces non-radiative recombination, and improves carrier confinement and injection efficiency. This leads to higher differential gain and enhances device temperature characteristics. Minimizing the series resistance of the laser is crucial for enhancing its performance. Lower series resistance delays the saturation of photocurrent characteristics, thereby improving laser output [8]. In addition, the cavity length of the laser greatly affects its output characteristics. A longer cavity can enhance thermal management by reducing the thermal resistance of the device, thereby increasing the maximum output power [9].

In this letter, we present a BH-DFB laser that utilizes AlGaInAs quantum well materials. By integrating additional groove structures, we effectively mitigate lateral current spreading, thereby enhancing current utilization. The laser features a low threshold current, exceptionally low RIN, and a high side mode suppression ratio (SMSR).

* Corresponding authors: hanjun@bjut.edu.cn (J. Han); tianyu.sun@hotmail.com (T. Sun).

We also explain the effects of various groove structures on the laser's series resistance. Additionally, we investigate the impact of chip temperature and cavity length on threshold current and slope efficiency.

2 Design and experiment

This study entailed the fabrication of an edge-emitting BH-DFB laser designed for operation at C-band wavelengths, specifically around 1550 nm. Figure 1 illustrates the structures of the laser diodes (LDs) employed in this investigation. The epitaxial layer was grown on an *n*-type InP substrate utilizing metal-organic chemical vapor deposition (MOCVD) technology. Initially, a 0.8-micron-thick *n*-doped InP buffer layer was grown, followed by the deposition of an active layer comprising multiple quantum well structures and separately restricted heterostructure (SCH). Then, the grating layer is grown. The mesa structure is formed through wet etching. Subsequently, *p*-InP and *n*-InP buried layers were grown to establish a current barrier. A layer of SiO_2 is grown on top of the wafer as a hard mask. Windows are opened in the silicon dioxide layer using reactive ion etching (RIE), and then wet etching is performed to form two different groove structures: a bowl-shaped groove structure based on isotropic etching and a vertical groove structure based on anisotropic etching. The etching depths of the two groove structures are roughly the same, as shown in Figure 2. After passivation, the SiO_2 dielectric layer was regrown and contact windows were etched using RIE. Then, a *p*-metal composed of Ti/Pt/Au is deposited and annealed to form ohmic contacts. Similarly, Ti/Pt/Au is grown on the thinned backside InP to form the *n*-side metal. Finally, the chips are cleaved according to different cavity lengths, and anti-reflection (AR) and high-reflection (HR) coatings are grown on the two end faces of each bar. The AR surface exhibited a reflectivity of 0.5%, while the HR surface boasted a reflectivity of 99%. Butterfly packaging was employed, and RIN testing was conducted subsequent to packaging.

Laser cross-sections were characterized using scanning electron microscopy (SEM). The current–voltage (I–V) curve of the ohmic contact interface was measured by a semiconductor parameter measuring instrument (4200-SCS/F+SUSS PM8). The laser output characteristic curve is measured by the laser LIV tester (XQT-LDBT-320). The optical power curves were plotted for different channel structures as well as for different cavity lengths. The output spectra at different temperatures were also plotted.

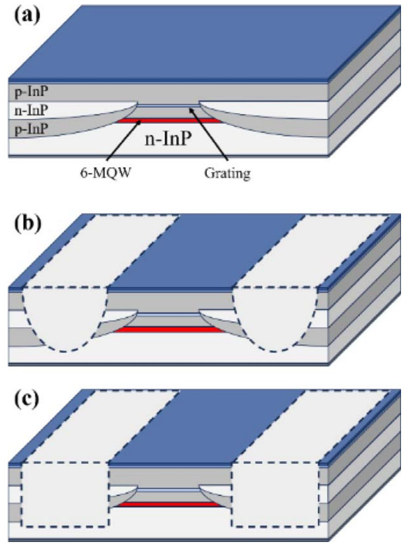

Fig. 1. Schematic diagrams of three types of LDs: (a) BH-DFB structure; (b) bowl-shaped groove BH-DFB structure; (c) vertical groove BH-DFB structure; the dotted line area is the groove structure.

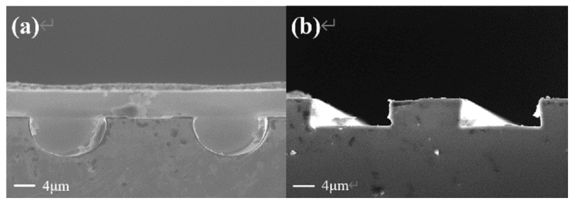

Fig. 2. SEM images of two groove structures: (a) bowl-shaped groove and (b) vertical groove.

3 Results and discussion

During the operation of semiconductor lasers, the connection between the laser and external circuits is primarily achieved through metal/semiconductor contacts [10]. With the ongoing miniaturization of lasers, leading to heightened current densities and temperatures within the active region, the demands placed on ohmic contacts are escalating [4]. Two fundamental prerequisites for ohmic contacts are low contact resistivity and high thermal stability. In this study, the ohmic contact performance was evaluated using the Ring Transmission Line Model. The semiconductor contact layer employed in this experiment was AlGaAs, while the metal contact layer consisted of Ti/Pt/Au. The outer radius of the ring transmission line model was set at 150 μm, with the minimum circular electrode radius being 60 μm, incremented by 10 μm. The inset in Figure 3 shows a SEM image of the actual ring transmission line model. After annealing at 425 °C for 125 s, voltage–current tests were conducted. Figure 3 illustrates the voltage-current test diagram of the ring transmission line model, where "r" denotes the spacing value between the two electrodes. It is evident from the figure that the current–voltage curves across all six sets of electrodes exhibit linearity. Upon calculation, the specific contact resistance is determined to be 4.61E−5 Ω*cm^2, with a corresponding contact resistance of 0.689 Ω*mm.

The ability of the buried structure to limit lateral diffusion current is provided by the electron potential barrier between the *pn* junctions within the buried structure, manifested as the "high-resistance region." The injected current, as shown in Figure 4, can be viewed as a parallel connection of three current components due to the unique "narrow

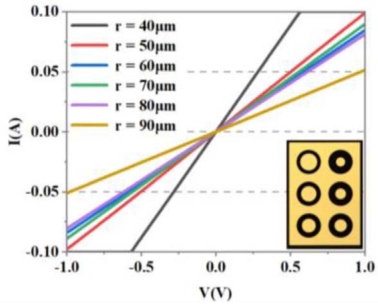

Fig. 3. Voltage–current test diagrams of Ring Transmission Line Model. Inset: SEM image of ring transmission line model.

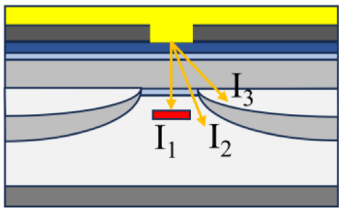

Fig. 4. The schematic diagram of injected current components in the buried structure.

stripe" structure of the BH laser active region (red area), As shown in formula (1).

$$I = I1 + I2 + I3 \tag{1}$$

Among them, I_1 represents the actual injected current into the active region; I_2 represents the leakage current between the buried structure and the active region when designing the BH laser; and I_3 represents the small amount of current leaking into the buried structure. Ideally, compared to I_1, I_2 and I_3 can be neglected. However, in reality, due to doping elements and process limitations, the leakage currents represented by I_2 and I_3 cannot be ignored and have a significant impact on the laser performance. Fortunately, we can control the size of I_3 by increasing the grooves, thereby reducing leakage current, that is, increasing the proportion of the I_1 current component in the injected current.

$$In = \frac{R_n}{R_1 + R_2 + R_3} \quad n = 1, 2, 3 \tag{2}$$

As indicated by formulas (1)–(2), we can reduce the current component leaking into the buried structure by increasing the resistance (R_3) of the buried structure. The resistance of the buried structure mainly comes from the *pn* junction barrier resistance, while the bulk resistivity of the material itself can be neglected. The barrier resistance of the *pn* junction is inversely proportional to the cross-sectional area of its interface. By adding groove structures to increase R_3, the principle mainly involves reducing the cross-sectional area of the current flowing through the buried *pn* junction.

In this study, both groove structures have the same top width of 15 μm, the width of the ridges between the grooves is also 15 μm, and the etching depths are approximately the same at 6 μm. However, due to the unique "bowl-shaped" structure, as the etching depth increases, the width of the ridges also increases. This implies that the cross-sectional area of the *pn* junctions in the buried structure also increases, leading to a decrease in the *pn* junction interface resistance and an increase in leakage current. We have demonstrated this in our experiments, as shown in figure below.

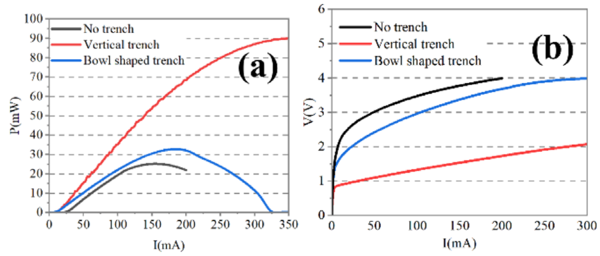

Fig. 5. (a) *P*–*I* curves of three LDs and (b) junction voltage curves of three LDs.

Figure 5a depicts the output power curves of lasers with different groove structures, while Figure 5b illustrates the curves of series voltage. From Figure 5b, it's evident that the series resistance of the "vertical-type" laser is halved compared to the "bowl-shaped" groove, stemming from the difference in the area of the *pn* junctions. This results in a stronger injection efficiency in the active region of the "vertical-type" laser, i.e., a larger I_1 component, leading to lower threshold current and higher slope efficiency. Moreover, the reduction in series resistance effectively postpones the saturation of the photocurrent characteristics. Considering these factors collectively, the lasers with "vertical-type" grooves exhibit a significant increase in measured output power, as depicted in Figure 5a.

The cavity length has a significant impact on the output characteristics of the laser. From formula (3) [11], it can be seen that a longer cavity brings more internal losses and results in lower slope efficiency.

$$P_0 = \eta_i \left(\frac{\alpha_m}{\langle \alpha_i \rangle + \alpha_m} \right) \frac{hv}{q} (I - I_{\mathrm{th}}) \ \ (I > I_{\mathrm{th}}) \tag{3}$$

η_i is the internal quantum efficiency, R_1 and R_{eff} is the reflectivity of the two end-face coatings, $\langle \alpha_i \rangle$ is the average internal loss, L is the cavity length, and I_{th} is the threshold current.

However, longer laser cavity offer several advantages. Firstly, longer cavity result in reduced mirror losses per unit cavity length on average, thereby lowering the threshold gain. Additionally, longer cavity enhance thermal management by reducing both device resistance and thermal resistance. This improved thermal management is crucial for maintaining stable laser performance and maximizing output power. Overall, longer cavity contribute to improving the efficiency and performance of lasers in various applications.

In this study, we fabricated three different cavity lengths of 800, 900, and 1000 μm utilizing a vertical groove structure. Notably, the 1000 μm cavity length exhibited the lowest threshold current of merely 4 mA and the highest output power (90 mW), as depicted in Figure 6.

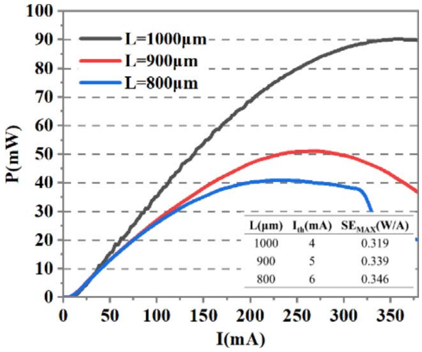

Fig. 6. P–I curves of vertical groove under different cavity lengths.

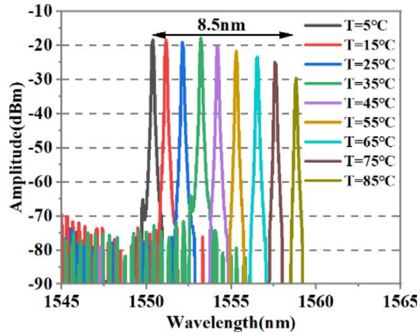

Fig. 7. Optical spectrums of a 1000 μm long vertical groove laser from 5 °C–85 °C at 400 mA.

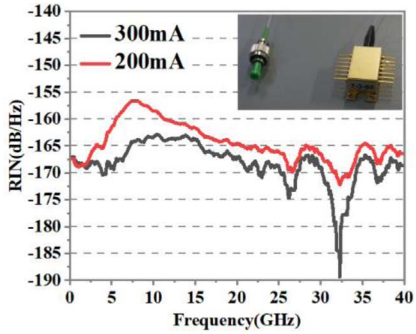

Fig. 8. RIN curves of 1000 μm long vertical groove laser under butterfly package at 200 mA (red) and 300 mA (black) current. Inset: real picture of butterfly after packaging.

This outcome is attributed to the beneficial effects of longer cavities, which contribute to the reduction of both electrical resistance and thermal resistance within the device, consequently leading to slower power saturation. However, it's important to note that despite these advantages, longer cavities also result in increased internal losses, which consequently lead to lower slope efficiency. This trade-off between threshold current, output power, and slope efficiency underscores the importance of optimizing cavity length based on specific application requirements.

The SMSR refers to the ratio between the output power of the main mode and that of the secondary mode when the laser is operating. It is an important indicator of the laser's stability in single-mode operation. A higher SMSR indicates that the laser's single-mode operation is more stable and the output spectrum is purer. According to Figure 7, our 1000 μm long vertical groove laser reaches peak power at a bias current of 400 mA, and the SMSR remains above 45 dB in the temperature range of 5 °C–85 °C. This indicates excellent single-mode stability and highlights its robust performance under different temperature conditions.

The SFDR denotes the power range over which microwave photonic links can transmit signals without distortion. In critical fields such as radar and electronic warfare, achieving a high SFDR in microwave photonic links is paramount. For instance, in anti-jamming radar systems, it's imperative that the SFDR of microwave photonic links reaches 120–130 dB·Hz$^{2/3}$ [12]. It is worth noting that the smaller RIN of the laser, the greater the SFDR of the microwave photonic link.

Intensity noise is commonly understood as the fluctuation in the quantified laser output power. While power fluctuations typically remain within 1% of their mean, in reality, there exists a smooth probability distribution with no sharp edges. To effectively address this, a root mean square (RMS) value is often specified. This approach is particularly applicable to relative power fluctuations, hence the specification of RIN [11].

$$\mathrm{RIN} \equiv \frac{\left\langle \delta P(t)^2 \right\rangle}{P_0^2} \tag{4}$$

RIN is represented by the output power spectral density and simplified to obtain the following formula [11]:

$$\frac{\mathrm{RIN}}{\Delta f} \approx \frac{2hv}{P_0}\left[\frac{\frac{\eta_0\eta_i(I+I_{\mathrm{th}})}{I_{\mathrm{st}}} + (1-\eta_0) + \omega^2\tau_p''^2}{1+\omega^2\tau_p''^2}\right] + \frac{2hv}{P_0}\frac{a_2\omega^2}{\omega_R^4}|H(\omega)|^2 \tag{5}$$

The formula's right side consists of two components: the first representing the background noise contribution, while the latter signifies the RIN peak resulting from damped resonance at the relaxation oscillation frequency. Increasing the output optical power shifts the peak to a higher frequency, resulting in a flat change in RIN. Formula (5) implies several key methods for minimizing laser RIN:

1. Improve the quantum well structure to achieve higher differential gain.
2. Increase laser output power to reduce RIN.
3. Lower RIN by reducing the threshold current.
4. Address uneven epitaxial quality or material defects.

Buried heterostructure lasers are known for exhibiting exceptionally low threshold currents, and incorporating groove structures can further enhance electron utilization.

In Figure 8, RIN curves for a 1000 μm vertical groove laser in a butterfly package are illustrated at 200 mA and 300 mA, with a TEC temperature of 25 °C. Remarkably, the RIN for this laser remains below −162.8 dB/Hz within the 0–40 GHz range at a working current of 300 mA.

4 Conclusion

In this work, we compares AlGaInAs buried heterostructure (BH) laser diodes using dual-channel ridge-waveguides with different groove shapes: bowl-shaped and vertical. In a vertical groove laser with a cavity length of 1000 μm, we have achieved a maximum output power of 90 mW and a threshold current as low as 4 mA. When the laser operated at a bias current of 400 mA, it achieved a SMSR greater than 45 dB within a temperature range of 5–85 °C. The laser's RIN in the 0–40 GHz frequency range is less than −162.8 dB/Hz when operated at 300 mA with the chip butterfly packaged. These findings demonstrate the superior performance of the developed DFB laser in terms of RIN, threshold current, and single-mode stability, highlighting its potential for microwave photonic link applications.

Acknowledgments

The authors would like to thank Nano Fabrication Facility, Platform for Characterization and Test, Chinese Academy of Sciences for their technical support.

Funding

Strategic Priority Research Program (B) of the Chinese Academy of Sciences (Grant No. XDB43030202) and National Key R&D Program of China (Grant No. 2022YFB2802500).

Conflicts of interest

The authors declare no conflicts of interest.

Data availability statement

Data underlying the results presented in this paper are not publicly available at this time but may be obtained from the authors upon reasonable request.

Author contribution statement

Jianhua Ren: Methodology, investigation, data curation, writing – original draft. Yanhui Xing: Methodology, visualization, writing – reviewing and editing. Jun Han: Methodology. Tianyu Sun: Conceptualization, methodology, writing – reviewing and editing. Zheng Xing: Methodology, supervision. Can Yin: Formal analysis. Baoshun Zhang: Resources, funding acquisition.

References

1 Ghelfi P., Laghezza F., Scotti F., et al. (2014) A fully photonics-based coherent radar system[J], *Nature* **507**, 7492, 341–345.

2 Lin J.W., Lu C.L., Chuang H.P., Kuo F.M., Shi J.W., Huang C.B., Pan C.L. (2012) Photonic generation and detection of W-band chirped millimeter-wave pulses for radar, *IEEE Photonics Technol. Lett.* **24**, 16, 1437–1439.

3 Ghelfi P., Onori D., Laghezza F., Scotti F., Bogoni A., Albertoni A., Tafuto A. (2015) An RF scanning receiver based on photonics for electronic warfare applications, in: *2015 European Radar Conference (EuRAD)*, IEEE, pp. 197–200.

4 Takaki K., Kise T., Maruyama K., Yamanaka N., Funabashi M., Kasukawa A. (2003) Reduced linewidth re-broadening by suppressing longitudinal spatial hole burning in high-power 1.55-μm continuous-wave distributed-feedback (CW-DFB) laser diodes, *IEEE J. Quantum Electron.* **39**, 9, 1060–1065.

5 Morton P.A., Morton M.J. (2018) High-power, ultra-low noise hybrid lasers for microwave photonics and optical sensing, *J. Lightwave Technol.* **36**, 21, 5048–5057.

6 Svetogorov V.N., Ryaboshtan Y.L., Ladugin M.A.E., Padalitsa A.A., Volkov N.A., Marmalyuk A.A.E., Slipchenko S.O., Lyutetskii A.V., Veselov D.A., Pikhtin N.A. (2020) AlGaInAs/InP semiconductor lasers with an ultra-narrow waveguide and an increased electron barrier, *Quantum Electron.* **50**, 12, 1123.

7 Higashi T., Sweeney S.J., Phillips A.F., Adams A.R., O'Reilly E.P., Uchida T., Fujii T. (1998) Observation of reduced non-radiative recombination current in 1.3-/spl mu/m AlGaInAs/InP multiple-quantum-well lasers, in: *Conference Digest. ISLC 1998 NARA. 1998 IEEE 16th International Semiconductor Laser Conference (Cat No. 98CH361130)*, IEEE, pp. 61–62.

8 Volkov N.A., Svetogorov V.N., Ryaboshtan Y.L., Andreev A.Y., Yarotskaya I.V., Ladugin M.A.E., Padalitsa A.A., Marmalyuk A.A.E., Slipchenko S.O., Lyutetskii A.V., Veselov D.A. (2021) Comparison of AlGaInAs/InP semiconductor lasers (λ = 1450–1500 nm) with ultra-narrow and strongly asymmetric waveguides, *Quantum Electron.* **51**, 4, 283.

9 Menna R., Komissarov A., Maiorov M., Khalfin V., DiMarco L., Connolly J., Garbuzov D. (2001) High power 1550 nm distributed feedback lasers with 440 mW CW output power for telecommunication applications, in: *Conference on Lasers and Electro-Optics*, Optica Publishing Group, p. CPD12.

10 Rideout V.L. (1975) A review of the theory and technology for ohmic contacts to group III–V compound semiconductors, *Solid-State Electron.* **18**, 6, 541–550.

11 Coldren L.A., Corzine S.W., Mashanovitch M.L. (2012) *Diode lasers and photonic integrated circuits*, John Wiley & Sons.

12 Merlet T., Formont S., Dolfi D., Tonda-Goldstein S., Vodjdani N., Auvray G., Blanc S., Fourdin C., Canal Y., Chazelas J. (2004) Photonics for RF signal processing in radar systems, in: *2004 IEEE International Topical Meeting on Microwave Photonics (IEEE Cat No. 04EX859)*, IEEE, pp. 305–308.